

Subharmonic frequency response in a magnetic pendulum

Yao Luo, Wenkai Fan, Chenghao Feng, Sihui Wang, and Yinlong Wang

Citation: American Journal of Physics **88**, 115 (2020); doi: 10.1119/10.0000038

View online: <https://doi.org/10.1119/10.0000038>

View Table of Contents: <https://aapt.scitation.org/toc/ajp/88/2>

Published by the American Association of Physics Teachers

AMERICAN
JOURNAL
of PHYSICS

Seeking applications for Editor
of the *American Journal of Physics* (AJP)





Subharmonic frequency response in a magnetic pendulum

Yao Luo

School of Physics, Nanjing University, Nanjing 210093, People's Republic of China

Wenkai Fan

Kuang Yaming Honors School, Nanjing University, Nanjing 210093, People's Republic of China and Department of Physics, Duke University, North Carolina 27710

Chenghao Feng

Kuang Yaming Honors School, Nanjing University, Nanjing 210093, People's Republic of China and Department of Electrical and Computer Engineering, The University of Texas at Austin, Texas 78712

Sihui Wang^{a)} and Yinlong Wang

School of Physics, Nanjing University, Nanjing 210093, People's Republic of China

(Received 20 April 2019; accepted 18 September 2019)

We study the subharmonic frequency response of a generalized driven oscillator excited by a nonlinear periodic force. We take a magnetic pendulum called the Doubochinski pendulum as an example. So-called “amplitude quantization,” i.e., the existence of multiple discrete periodic solutions, is identified as subharmonic resonance in response to nonlinear feeding. The subharmonic resonance frequency is found to be related to the symmetry of the driving force: Odd subharmonic resonance occurs under an even symmetric driving force, and vice versa. We obtain multiple periodic solutions and investigate the transition and competition between multistable orbits via frequency response curves and Poincaré maps. Experimentally observed phenomenon can easily be reproduced in a student laboratory. This provides a perfect example to demonstrate the rich dynamics related to the effect of nonlinear driving within the scope of undergraduate physics. © 2020 American Association of Physics Teachers.

<https://doi.org/10.1119/10.0000038>

I. INTRODUCTION

In oscillatory systems, nonlinear phenomena arising from restoring forces^{1–7} are often encountered. For example, a Duffing oscillator containing a cubic term in the restoring force exhibits typical nonlinear behavior such as a hardening or softening frequency response, a “jump” phenomenon and hysteresis, bistability, symmetry-breaking bifurcations, and chaotic motion.^{4–7} Nonlinearity arising from damping has also received attention in recent years.^{8–11} In addition, various experimental devices have been created to demonstrate nonlinear behavior to undergraduates.^{6–8,12,13}

In this paper, we introduce the nonlinear effects on a pendulum to which a nonlinear periodic driving force is applied, taking the Doubochinski magnetic pendulum as an example. The Doubochinski pendulum¹⁴ is a rigid pendulum with a small magnet at its free end driven by an AC-powered electromagnet underneath. A remarkable feature of the system is that it performs stable oscillations at large discrete amplitudes in what is called “amplitude quantization.”^{14–16} Damgov and Popov¹⁷ called such system a kick-excited one: Since the intensity of the magnetic field generated by the AC-powered coil decreases dramatically with increasing displacement, the driving force acts on a small region and is negligible elsewhere. They studied a system with a Π-shaped feeding function and discovered that it exhibits strong self-adaptivity; that is, the amplitude of oscillation is insensitive to the amplitude of the driving force. Recently, Cintra *et al.* explored the dynamical properties of a similar system both experimentally¹⁸ and theoretically.¹⁹

We reveal that the mysterious “amplitude quantization,” initially studied as “macroscopic quantum behavior,”¹⁴ is in fact a subharmonic resonance in response to the nonlinear driving force $f(x) \cos \omega t$, where ω is the driving frequency and the feeding function $f(x)$ is a nonlinear function of displacement.

A resonance that occurs when the driving frequency is close to an integer multiple of the natural frequency is called a subharmonic resonance.

A typical example of subharmonic resonance is the linear parametric oscillator governed by the Mathieu equation.^{20,21} “Parametric resonance” occurs when the driving frequency is in the vicinity of an even multiple of the natural frequency and subharmonic resonance is observed. From daily experience, we know that a child on a swing can drive the swing to higher amplitudes by appropriate modulation of the system parameters (e.g., by adjusting the center of mass) twice a cycle.^{22,23} In the Mathieu equation, the driving term $x \cos(\omega t)$ contributes to principal parametric resonance at $\omega = 2\omega_0$, where ω_0 is the natural frequency of the pendulum.

The subharmonic resonance in the Doubochinski pendulum can be regarded as characteristic of generalized parametric oscillation. We will find that the subharmonic resonant frequency is related to the symmetry of the feeding function (under inversion of angular displacement: $\theta \rightarrow -\theta$): odd subharmonic resonance occurs for even symmetric $f(x)$, and vice versa.

To understand the mechanism of subharmonic resonance, we consider an even symmetric feeding function $f(x)$ and express $f(x)$ as a series of polynomials, solving for the multiple discrete orbits and frequency response curves analytically near $\omega = 3\omega_0$. Thus, the origin of multiple discrete orbits and strong self-adaptivity can be explained.

Multiple stable orbits near $\omega = 3\omega_0$ and $\omega = 5\omega_0$ are studied numerically. To investigate the transition and competition between multiple orbits on subharmonic resonance, we present the frequency response curves and Poincaré maps near $\omega = 3\omega_0$ and $\omega = 5\omega_0$. The transition between multistable orbits is more complex and intriguing than in the case of bistability. We find an irreversible transition between the multistable states and propose a multistability control

strategy. In contrast, the frequency response for bistable states forms a closed hysteresis loop rather than an open path.

This problem aroused extensive interest among undergraduates and even high school students as a popular competition problem in the 2015 International Young Physicists' Tournament and 2015 China Undergraduate Physics Tournament.^{24–26} It also provides an example of the phenomenon of multistability (i.e., the coexistence of different attractors for a given set of parameters) that is widespread in physics,^{28–30} chemistry,^{31,32} biology,^{33–35} and elsewhere in science and nature. The phenomenon can easily be reproduced experimentally in a student laboratory.²⁶ It provides a perfect example to demonstrate, within the scope of undergraduate physics, the rich dynamics associated with the effects of nonlinear driving.

II. THEORETICAL MODEL

A. Dynamic equation

The general form of a nonlinearly excited oscillator can be described by the following dynamical equation:

$$\ddot{x} + 2h\dot{x} + f_r(x) = f(x) \cos \omega t, \quad (1)$$

where x is the displacement, h is the linear damping coefficient, $f_r(x)$ is the restoring force of the system, $f(x) \cos \omega t$ is a nonlinear periodic driving force, and ω is the driving frequency. $f(x)$ is the displacement-dependent amplitude of the driving force, called the feeding function here. There are various physical systems that are described by equations of similar form. For example, when $f_r(x)$ contains a positive linear term and a cubic term, and the feeding function $f(x)$ is a constant, Eq. (1) becomes the Duffing equation.⁴ A nonlinear parametric oscillator is described by an equation similar to Eq. (1) in which $f(x)$ also contains linear and cubic terms.³⁶

When applied to a pendulum, the restoring force can be written as

$$f_r(x) = \omega_0^2 \sin x, \quad (2)$$

where ω_0 is the natural frequency of the pendulum and x is the angular displacement.

The actual form of the feeding function is complicated, so we approximate it in terms of polynomials of x to allow us to perform analytical calculations. Specifically, if $f(x)$ is an even symmetric function of x , then the polynomial approximation contains only terms of even degree

$$f_{\text{even}}(x) = a_0 + a_2 x^2 + a_4 x^4 + \dots \quad (3)$$

If $f(x)$ is an odd symmetric function of x , then the approximation contains only terms of odd degree

$$f_{\text{odd}}(x) = a_1 x + a_3 x^3 + \dots \quad (4)$$

In many cases, the feeding function $f(x)$ has large values in an active zone and becomes negligible elsewhere; such a pendulum is called a “kick-excited” one. Damgov and Popov¹⁷ considered a symmetric Π -shaped feeding function. Here, the polynomial series is truncated after the lowest few terms to model the feeding function. The coefficients are determined by fitting $f(x)$ of a particular physical model using the above polynomials. Since the polynomial usually

fails to converge to the practical feeding function for arbitrary displacements, the polynomial approximation applies only to the range of oscillation or the “active zone” of the feeding function.

B. Feeding function for a magnetic pendulum

In the following, we consider a practical model of a nonlinearly excited oscillator, the Doubochinski pendulum. This consists of a light rigid pendulum with a small magnet at the free end. An AC-powered electromagnet is placed vertically or horizontally beneath the pendulum; see Figs. 1(a) and 1(b). The direction of the poles of the magnet are adjusted to lie along the local geomagnetic field to eliminate torque. The dynamical equation of the pendulum is

$$\ddot{x} + 2h\dot{x} + \omega_0^2 \sin x = \frac{T(x)}{I} \cos \omega t, \quad (5)$$

where I is the moment of inertia of the pendulum and $T(x)$ is the torque applied to the magnet fixed at the lower end of the pendulum. We can write the dynamical equation in dimensionless form as

$$\frac{d^2x}{d\tau^2} + 2\beta \frac{dx}{d\tau} + \sin x = f(x) \cos \Omega \tau, \quad (6)$$

where τ , β , and $f(x)$ are defined as

$$\tau = \omega_0 t, \quad \beta = \frac{h}{\omega_0}, \quad (7)$$

$$f(x) = \frac{T(x)}{I\omega_0^2}, \quad \Omega = \frac{\omega}{\omega_0}. \quad (8)$$

The driving term arises from the alternating magnetic field. The torque can be evaluated by treating the magnet as a magnetic dipole

$$T(x) = \frac{\partial(MB)}{\partial x}, \quad (9)$$

where B is the magnetic induction of the field and M is the magnetic moment of the magnet. Here, we calculate the feeding function in two typical configurations. The parameters to be used in the numerical calculation are given in Table I: the natural frequency of the pendulum ω_0 , its moment of inertia I , its length L , the radius of the coils r , the number of turns N , the height of the electromagnet coil H , the distance between the coil and the magnet d , the magnetic moment of the magnet M , and the current i . The table also gives the coefficients a_0 , a_2 , and a_4 of the polynomial in Eq. (3) fitted to the feeding function given by these above parameters. These coefficients will be used in the analytical calculation. As shown in Figs. 1(c) and 1(d), when the electromagnetic coil is placed vertically, $f(x)$ has even symmetry; when the coil is placed horizontally, $f(x)$ has odd symmetry.

III. DYNAMICAL BEHAVIOR

A. Discrete periodic orbits

The motion of the pendulum is governed in Eqs. (6) and (9). We solve these equations for the case in which the electromagnet is placed vertically, using the feeding function

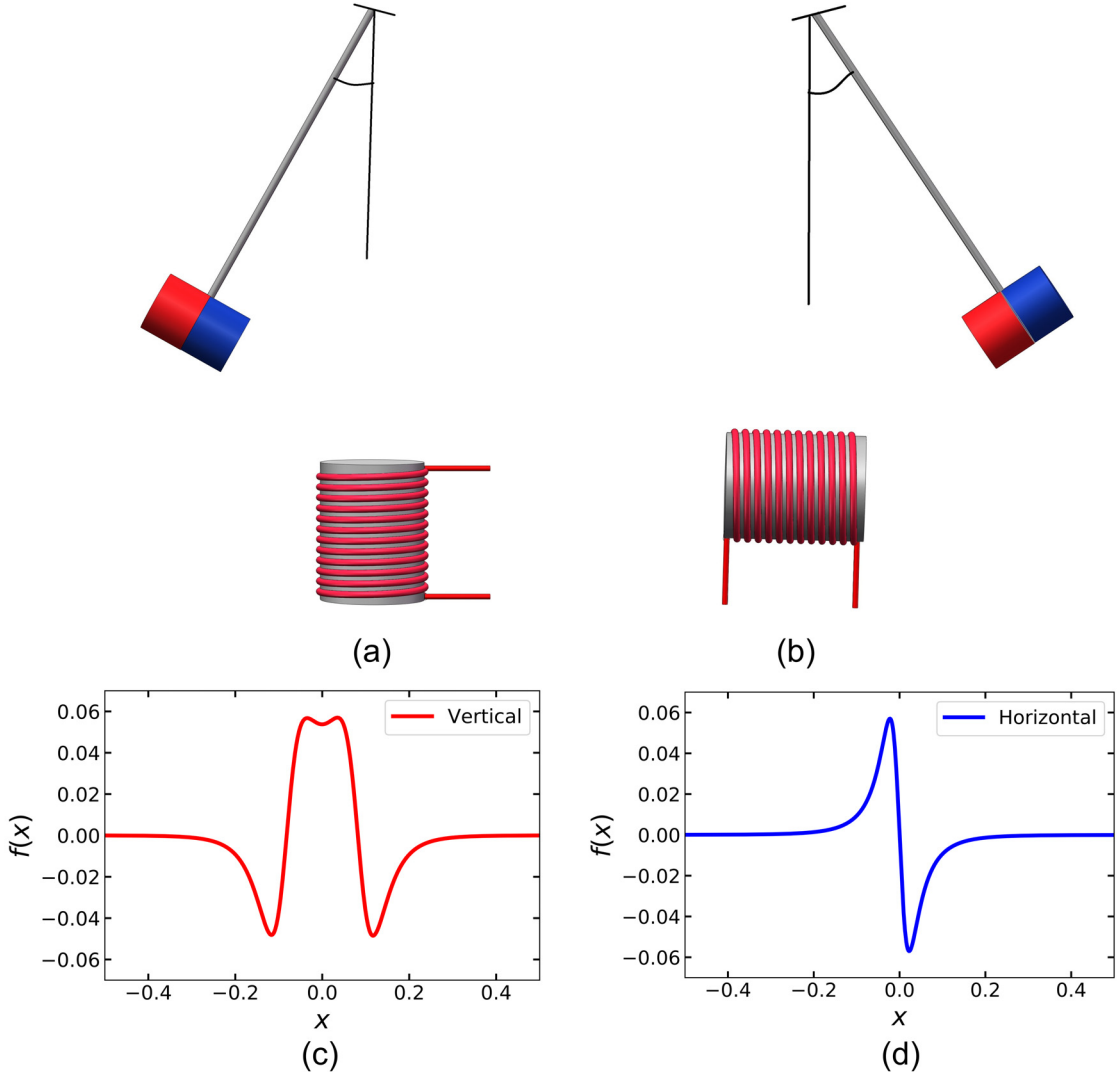


Fig. 1. (a) and (b) are schematic diagrams of the Doubochinski pendulum with the electromagnet placed vertically and horizontally, respectively. (c) and (d) show the corresponding feeding functions $f(x)$ versus the angular displacement x .

shown in Fig. 1(c) and the fourth-order Runge–Kutta method in C++.

From Fig. 2, we can see that there are several stationary oscillation modes near frequencies that are three and five times the natural frequency ($\Omega = 2.98$ and $\Omega = 4.98$, respectively). Figures 2(a) and 2(b) show the time evolution of typical periodic orbits. The final oscillation modes are dependent on initial

Table I. Parameters used to calculate the feeding function, and the fitting coefficients of the polynomial in Eq. (3).

Parameters	ω_0 (rad/s)	I (kg m^2)	L (m)	r (m)	N
	5.13	0.01	0.456	0.042	220
H (m)	d (m)	M (A m^2)	i (A)	β (rad/s)	
0.02	0.021	1.36	0.5	0.0156	
Fitting coefficients	a_0	a_2	a_4		
0.055	-11.6	300			

conditions. We then sample the initial condition in phase space (x, \dot{x}) , in search of stable oscillation orbits. All the trajectories converge to several limit cycles, as shown in Figs. 2(c) and 2(d). The small cycles in the middle are the linear solutions where the pendulum oscillates at the frequencies of the driving force. The larger cycles are nonlinear solutions where the pendulum oscillates near the natural frequency. The insets in Figs. 2(c) and 2(d) show the dual stationary solutions corresponding to the larger limit cycles. Although the two limit cycles are adjacent in the phase diagram, they differ in phase. From Fig. 2, we also see that for the large stationary solutions, the pendulum approximately performs harmonic oscillations.

These results are consistent with the experimentally observed phenomenon²⁶ that a pendulum released at small angles performs only small oscillations in the “linear region,” while for larger angles of release, the amplitude varies slowly and ends up with stable harmonic oscillations on large-amplitude orbits or a small linear orbit. The values of the parameters are chosen to match the experimental feeding function and thereby allow comparison with experimental results. In our theoretical approach, when $\Omega \approx 3$, the larger oscillation has a pair of separated orbits with amplitudes around 0.18.

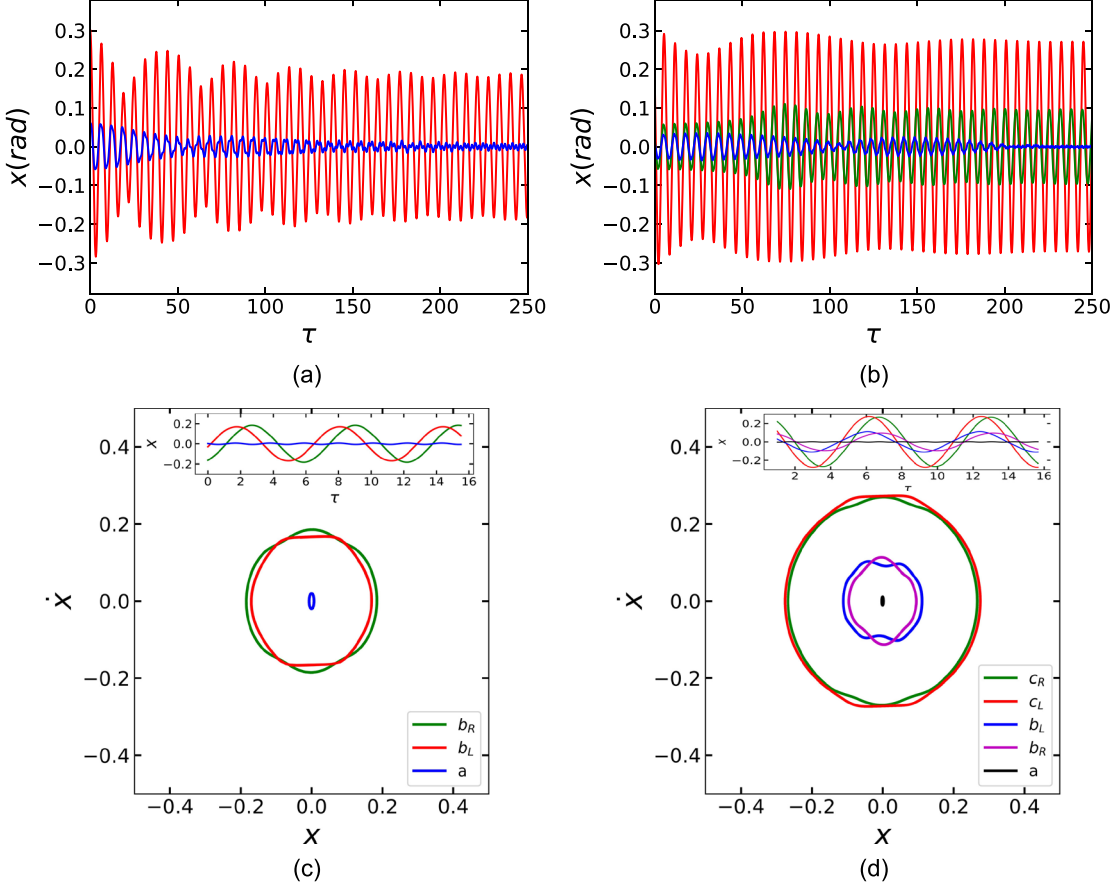


Fig. 2. (Color online) (a) and (b) show multiple stationary solutions of the Doubochinski pendulum for driving frequency $\Omega = 2.98$ and 4.98 , respectively. The final oscillation modes depend on initial conditions. The corresponding limit cycles are shown in (c) and (d), respectively. x , \dot{x} , and τ are the angular displacement, dimensionless angular velocity, and dimensionless time, respectively. The small cycles in the middle are the linear solutions. The larger cycles that appear in pairs are nonlinear solutions where the pendulum oscillates near the natural frequency. The insets show stationary solutions of the corresponding limit cycles in the same color. See Sec. III D for an explanation of a , b_L , b_R , c_L , and c_R .

Experimentally, the amplitude of the larger oscillation is found to be about 0.22. A possible source of this discrepancy might be that the dual orbits are not distinguished in the experiment.

B. Analytical results for the frequency response curves

To find the multiple periodic solutions analytically, we use the polynomial approximation of the feeding function in Eq. (3) and truncate it after fourth order.

In Eq. (3), when $x \ll 1$, the leading term is a constant a_0 . The pendulum performs only regular linear forced oscillations at the driving frequency. At larger angles, the effect of nonlinearity becomes significant. When the pendulum performs large-amplitude oscillations near $\Omega = 3$, the zeroth solution of Eq. (6) should be written as

$$x_0 = A \cos\left(\frac{\Omega}{3}\tau + \phi\right). \quad (10)$$

To find out how the amplitude changes with driving frequency in the vicinity of $\Omega = 3$, a detuning parameter σ is introduced as follows:

$$\Omega = 3(1 + \sigma). \quad (11)$$

σ measures the closeness of the driving frequency to the sub-harmonic resonance condition.

We then apply the averaging method.^{19,27} This method is based on the assumption that the motion of an oscillator can be approximated as a near-harmonic oscillation with slowly varying amplitude and phase. With this assumption, higher-order time derivatives of the amplitude and phase are neglected, with only the first-order time derivatives being retained. Substituting Eq. (10) into Eq. (6) and averaging the amplitude and phase changes over one period, we obtain the time derivatives of the amplitude and phase

$$\dot{A} = -\frac{2A\beta}{1+\sigma} - \frac{A^2(4a_2 + 3a_4A^2)\sin(3\phi)}{16(1+\sigma)}, \quad (12)$$

$$\dot{\phi} = -\frac{A^2 + 16\sigma}{8(1+\sigma)} - \frac{A(4a_2 + 5a_4A^2)\cos(3\phi)}{16(1+\sigma)}. \quad (13)$$

For simplicity, we set the damping coefficient $\beta = 0$. These two equations give an approximate description of the motion of the oscillator in (A, ϕ) space. The stationary solutions are the fixed points in (A, ϕ) space, which satisfy

$$\dot{A} = 0, \quad \dot{\phi} = 0. \quad (14)$$

The solutions are then

$$4a_2A + 5a_4A^3 = 32\sigma + 2A^2, \quad \phi = (2n+1)\frac{\pi}{3}, \quad (15)$$

$$4a_2A + 5a_4A^3 = -32\sigma - 2A^2, \quad \phi = 2n\frac{\pi}{3}, \quad (16)$$

in which $n \in \mathbb{Z}$. The term $2A^2$ can be ignored henceforth because it is much smaller than a_2A and a_4A^3 ; see Table I. When $\sigma = 0$, the amplitudes found from Eqs. (15) and (16) are the same

$$A = \pm \sqrt{\frac{-4a_2}{5a_4}}, \quad 0. \quad (17)$$

Equation (17) indicates that nontrivial stationary solutions exist when a_2 and a_4 are different in sign. Here, multistability is achieved without dissipation when the polynomial of the feeding function contains more than one nonlinear term, so energy balance can be realized.³⁷ A feeding function truncated after fourth order can produce resonance at $\Omega \approx 3$. For higher subharmonic frequencies, a feeding function with higher-order terms needs to be considered.

The oscillation amplitudes in Eq. (17) are independent of the amplitude of the driving force, since the coefficients a_2 and a_4 are both proportional to the current intensity in the coils (or the amplitude of the driving force), so the ratio will not change with the amplitude of driving force. Such strong self-adaptivity has been verified both in computations¹⁷ and experimentally,²⁶ where it has been found that the amplitudes remain almost unchanged when the driving force varies over a very large range. Actually, when the amplitude of the driving force exceeds a critical value, the oscillator will undergo a series of symmetry-breaking oscillation modes with multiple periods and will finally become chaotic. The period-3 bifurcations in a system with Π -shaped feeding function reported by Damgov and Popov¹⁷ provide a similar example.

The frequency response curves shown in Fig. 3 can be obtained from Eqs. (15) and (16) when $\sigma \neq 0$. The nonlinear solutions contain one small unstable root, denoted by the blue dashed curve, and a pair of large stable roots, denoted by the black solid curves, and this is independent of n in Eqs. (15) and (16). The origin of this degeneracy is that the period of the oscillator is three times that of the driving force. Thus, two oscillations with $2\pi/3$ phase difference experience the same driving force. They are released with the same initial angular displacement and velocity, but one begins oscillating

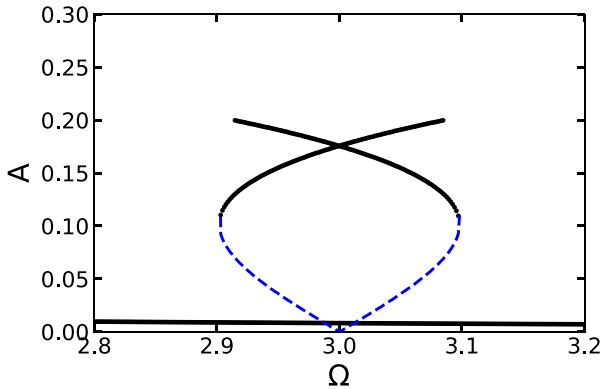


Fig. 3. Analytical results for the amplitude frequency response curves for dimensionless driving frequency $\Omega \approx 3$. A is the oscillation amplitude. The two black solid curves denote the larger stable roots and the blue dashed curve the unstable root. The linear forced oscillation solution is the solid line near the bottom.

with one period of the driving force earlier than the other. The linear forced oscillation solution is also plotted as the solid line near the bottom of Fig. 3.

C. Symmetry of the driving force and frequency response

To clarify how the symmetry of the feeding function influences the subharmonic frequencies, we calculate the overall frequency response for even symmetric and odd symmetric $f(x)$. In the calculation, we consider damping and use Eq. (9) and the parameters listed in Table I to model the feeding function and solve numerically to obtain the frequency response diagram. Since multiple periodic oscillation modes coexist when subharmonic resonance occurs, we show only the maximum amplitudes on the frequency response diagram.

In Fig. 4, the dotted-dashed curves correspond to the solutions for the even symmetric feeding function and solid curves to those for the odd symmetric feeding function. We find that subharmonic resonance occurs for $\Omega \approx 2k - 1$ and $\Omega \approx 2k$ in response to even and odd symmetric feeding functions, respectively, with $k \in \mathbb{N}$ and $k \geq 2$. Since an asymmetric function can be decomposed into an odd function and an even function, we can infer that if the electromagnet is placed in an inclined position, then subharmonic resonance should occur for $\Omega \approx k$.

D. Mode competition

A Duffing oscillator with cubic nonlinearity in the restoring force exhibits a jump phenomenon and hysteresis between bistable states owing to hardening or softening resonance.⁴ The hardening (softening) frequency response happens when the resonant peak leans toward higher (lower) frequency owing to nonlinearity that strengthens (weakens) the restoring force as the displacement increases. For a nonlinear parametric oscillator, the frequency response curves exhibit mixed feature of softening and hardening.³⁶ Here, a more complex jump phenomenon, induced by mode competition among multiple attractors, is studied.

To study the transition behavior among the attractors, the frequency response graph is calculated when the driving frequency increases or decreases quasistatically. Figure 5(e) shows the frequency response diagram when $\Omega \approx 3$. Similar

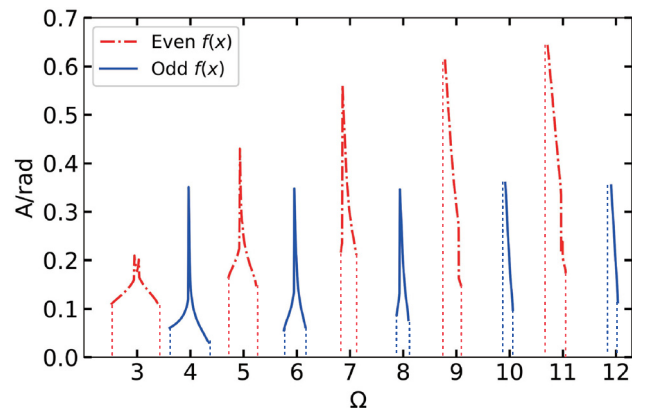


Fig. 4. (Color online) The maximum amplitude frequency response diagram. A and Ω are the amplitude of oscillation and the dimensionless driving frequency, respectively. The red (dotted-dashed) and blue (solid) curves are for even and odd feeding functions, respectively. Subharmonic resonance occurs for $\Omega \approx 2k - 1$ and $\Omega \approx 2k$ in response to even and odd feeding functions, respectively. The frequency response curve for linear forced oscillations is not plotted.

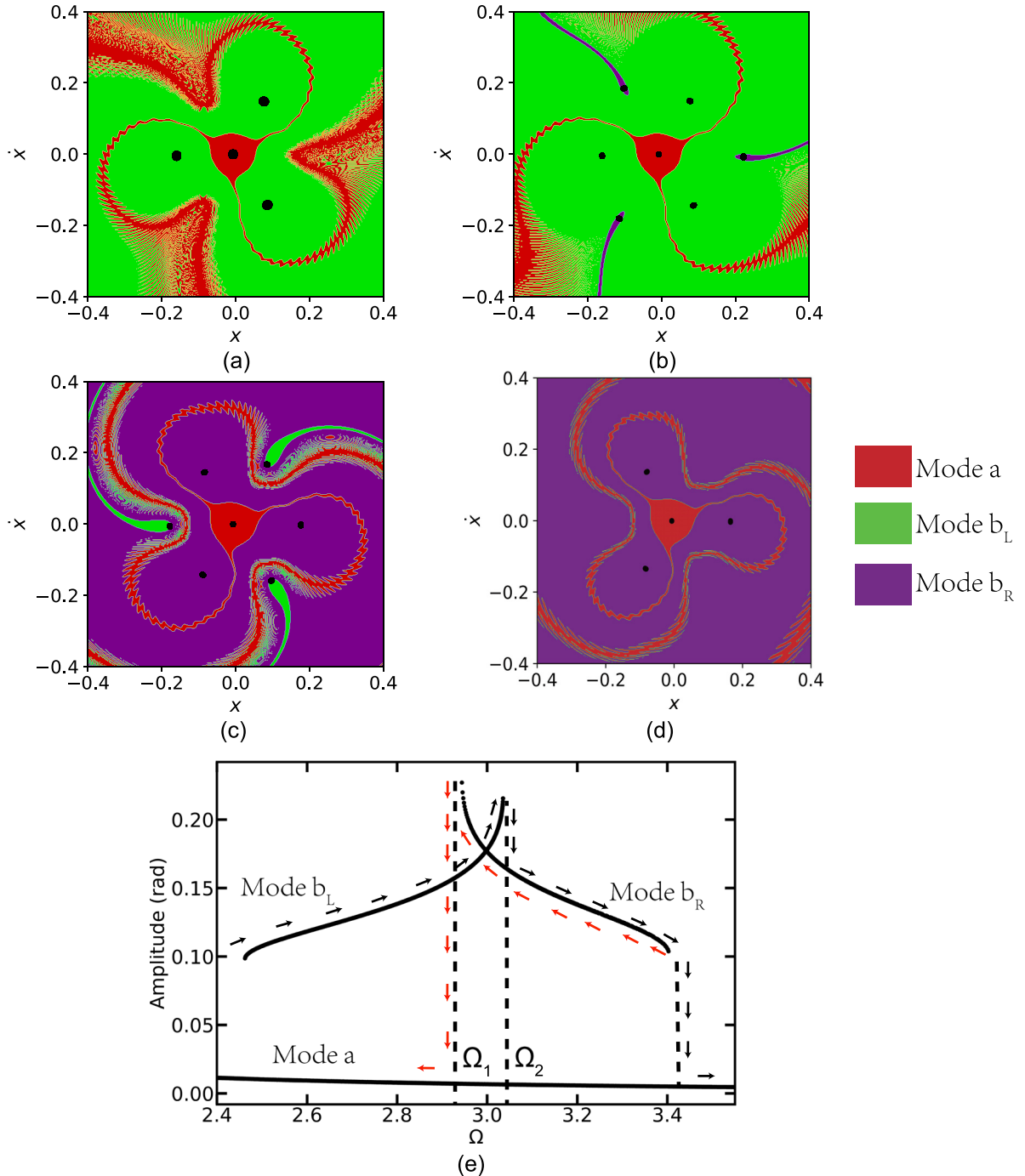


Fig. 5. (Color online) (a)–(d) show the evolution of the basins of attraction in Poincaré maps for $\Omega = 2.940, 2.945, 3.000$, and 3.040 , respectively. x and \dot{x} are the angular displacement and dimensionless angular velocity, respectively. The black dots are the fixed points (FPs) for each basin. The basins of attraction for FPs of modes a , b_L , and b_R are shown by the light grey (red), light grey (green), and dark grey (purple), respectively. (e) Frequency response curves for $\Omega \approx 3$, where mode a is the linear oscillation mode with the driving frequency and the modes b are the large oscillation modes with oscillation frequency near the natural frequency. The arrows beside the curves indicate how the oscillation modes evolve with driving frequency. The critical frequencies are $\Omega_1 = 2.943$ and $\Omega_2 = 3.020$.

to the analytical result in Fig. 3, for $\Omega \approx 3$ it has a small linear solution, called mode a , and a pair of overlapping branches, called modes b_R and b_L , which correspond to the three stable orbits in Fig. 2(c) (L and R stand for “left” and “right”). The unstable solutions are not presented here, since they are unavailable via numerical integration of Eq. (6).

Transition occurs when one orbit loses stability and the oscillator jumps to another orbit, as the control parameter, i.e., the driving frequency, changes quasistatically. In Fig. 5(e), the arrows beside the frequency response curves

indicate how the transition takes place. The frequency condition for all stationary modes b_R , b_L , and a to coexist is $\Omega_1 \leq \Omega \leq \Omega_2$. When $\Omega \leq \Omega_1$, modes b_L and a are stable, and when $\Omega > \Omega_2$, modes b_R and a are stable. As the frequency increases, the oscillator in mode b_L jumps to mode b_R at $\Omega = \Omega_2$. Unexpectedly, as the frequency decreases, a transition occurs from mode b_R to mode a at $\Omega = \Omega_1$. We see that the transition shows irreversible characteristics. It is the coexistence of multiple attractors that makes such an irreversible transition possible.

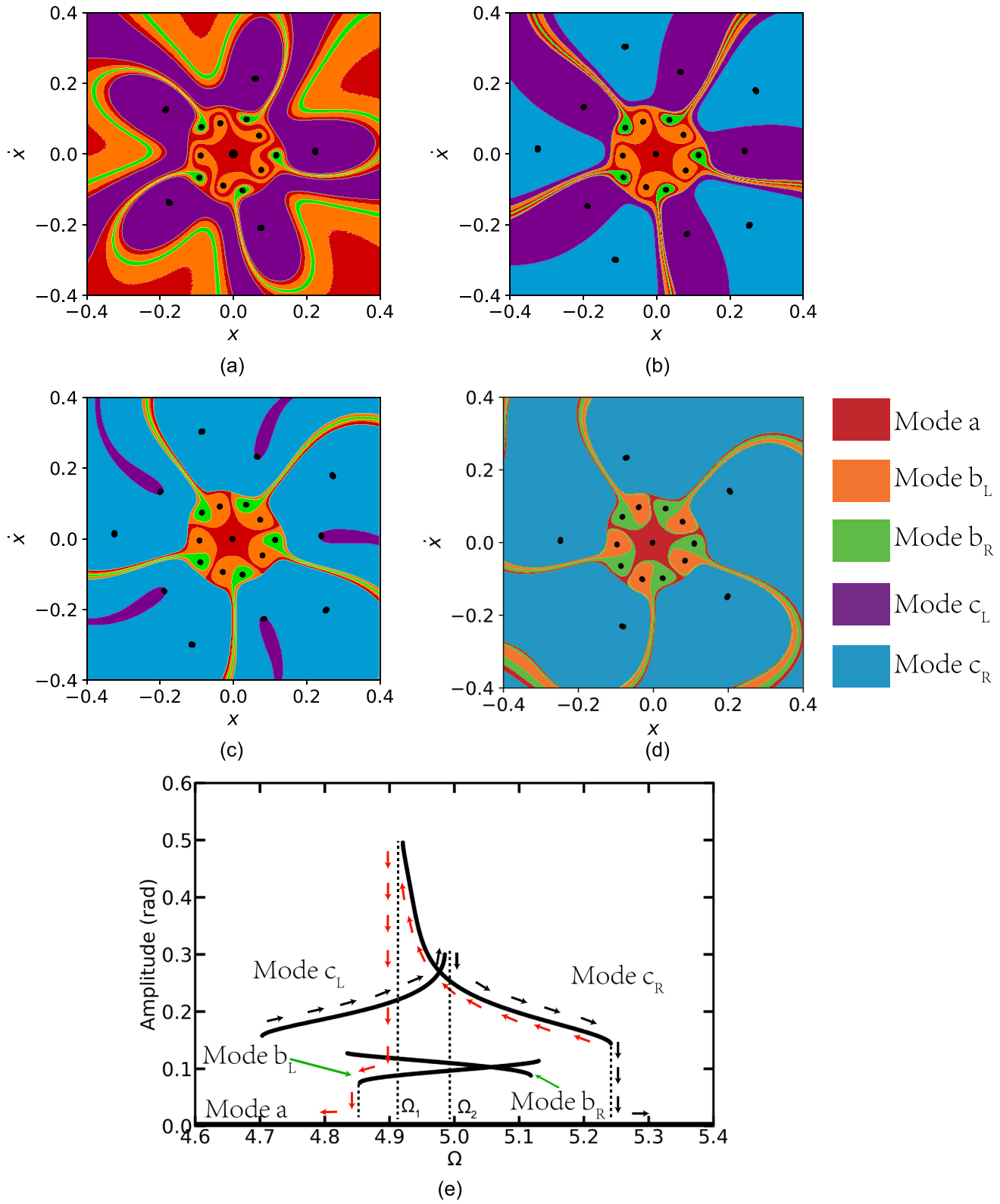


Fig. 6. (Color online) (a)–(d) show the evolution of the basins of attraction in Poincaré maps for $\Omega = 4.92, 4.95, 4.98$, and 5.0 , respectively. The black dots are FPs for each basin. The basins of attraction for each FP are denoted by different colors. The basin in the middle (red) is mode a . The lighter grey (orange) and darker grey (green) are the basins for modes b_L and b_R , respectively, which are the lower pair like snakes. The dark grey (purple) and light grey (blue) higher basins in pair represent those for modes c_L and c_R , respectively. (e) Frequency response curves for $\Omega \approx 5$. The arrows beside the curves indicate how the oscillation modes evolve with driving frequency. The critical frequencies are $\Omega_1 = 4.93$ and $\Omega_2 = 4.99$.

This irreversible transition behavior can be described in terms of the evolution of basins of attraction in Poincaré maps. Figures 5(a)–5(d) show these basins for $\Omega = 2.94, 2.945, 3.0$, and 3.04 , respectively. In each figure, the small

black dots are fixed points (FPs). Each FP is surrounded by its basin of attraction, indicated in color. The light grey (red), light grey (green), and dark grey (purple) areas denote the basins of attraction for modes a , b_L , and b_R , respectively.

Mode a (the linear oscillation mode with oscillation frequency equal to the driving frequency) leaves one fixed point near the center in Figs. 5(a)–5(d). Meanwhile, each large-amplitude mode has three fixed points, because the oscillation periods of modes b_R and b_L are three times the period of the driving force.

In Figs. 5(b)–5(d), as the driving frequency increases from $\Omega = 2.945$ to 3.00 and 3.040, the basin of attraction of b_L shrinks quickly and vanishes below 3.040. In Fig. 5(c), just below the transition frequency, the vanishing basins of attraction of b_L surrounded by those of b_R merge into those of b_R , and a transition from b_L to b_R occurs.

In Figs. 5(b) and 5(a), in the vicinity of the critical frequency Ω_1 , the basins of attraction of b_R are surrounded by those of mode a [the light grey (red) area]. As the driving frequency decreases from 2.945 to 2.940, the basins of mode b_R are replaced by those of mode a , so a transition from mode b_R to a occurs. The evolution of the basins of attraction is responsible for the transition from mode b_R to mode a and explains the irreversible characteristics.

In addition, the frequency response diagram and Poincaré maps for $\Omega \approx 5$ are shown in Figs. 6(a)–6(e). The five stable orbits in Fig. 2(d) correspond to a single linear branch, called a , and two pairs of overlapping branches, called b_L , b_R , c_L , and c_R , in Fig. 6(e). Ω_1 is the lower critical frequency for mode c_R , and Ω_2 is the upper critical frequency for mode c_L . In Figs. 6(a)–6(d), the basins of attraction of modes a , b_L , b_R , c_L , and c_R are presented. Below, we focus mainly on a typical transition starting from modes c_L and c_R .

Figure 6(e) shows that transitions among different modes are again irreversible. When the driving frequency is increased, the oscillator at mode c_L will jump to mode c_R at $\Omega = \Omega_2$. In Fig. 6(c), the basins of attraction of mode c_L are surrounded by those of c_R below Ω_2 , and the basins of c_L merge into that of c_R when the driving frequency exceeds Ω_2 ; see Fig. 6(d).

As the driving frequency is decreased, the oscillator at mode c_R jumps to mode b_L at $\Omega = \Omega_1$, rather than to c_L . In Figs. 6(b) and 6(a), the basins of attraction of mode c_R merge into that of mode b_L below Ω_1 .

From the transition sequence described in Figs. 5(e) and 6(e), we propose a control strategy among the oscillation modes by adiabatically changing the driving frequency. For example, in Fig. 5(e), starting from mode b_L , the oscillator can be induced to change to mode b_R by increasing the driving frequency, and then to mode a by decreasing the driving frequency. However, a transition from mode a to higher oscillation modes is unlikely to happen. This means that an oscillator initially performing linear oscillations in mode a cannot be driven to higher orbits merely by changing the driving frequency.

IV. CONCLUSION

We have investigated the subharmonic frequency response of a generalized nonlinear forced oscillator excited by $f(x) \cos \omega t$, taking the Doubochinski pendulum as an example. We have expressed the energy feeding function as a polynomial and found that subharmonic resonance of discrete stationary orbits can be achieved when the polynomial contains more than one nonlinear term so that energy balance can be realized. We have also found the subharmonic resonance frequency conditions and have demonstrated the

correspondence between the symmetry of the feeding function and the subharmonic resonance frequencies.

The nonlinear behavior studied in this paper includes self-adaptive oscillation, subharmonic frequency resonance, and irreversible transition between multistable states. This behavior also helps to understand the phenomena of multistability that are widespread in many fields of science and nature.

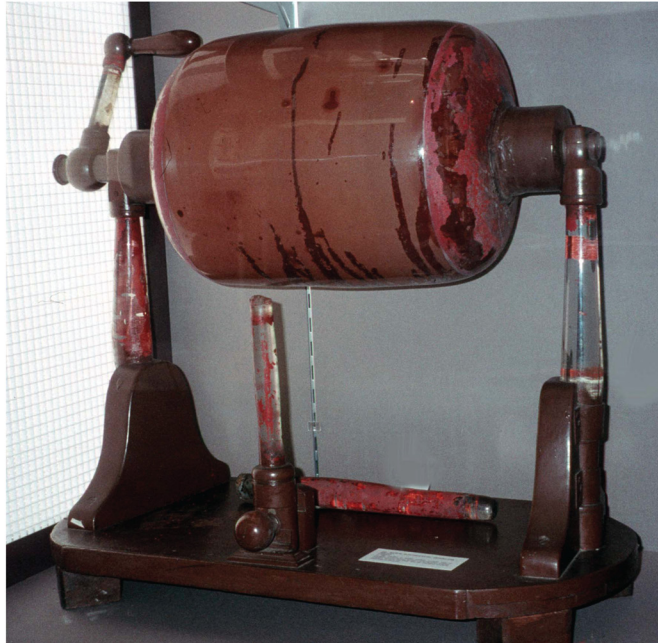
ACKNOWLEDGMENTS

The authors are grateful to Professors Xiaoshan Wu and Jianguo Wan from Nanjing University and our friend Mr. Li Du from Massachusetts Institute of Technology for helpful discussions. Y. Luo would like to extend sincere thanks to his roommate Mr. Jiahao Dong for computational resources.

^{a)}Electronic mail: wangshui@nju.edu.cn

- ¹P. Mohazzabi, “Theory and examples of intrinsically nonlinear oscillators,” *Am. J. Phys.* **72**(4), 492–498 (2004).
- ²A. Siahmakoun, V. A. French, and J. Patterson, “Nonlinear dynamics of a sinusoidally driven pendulum in a repulsive magnetic field,” *Am. J. Phys.* **65**(5), 393–400 (1997).
- ³P. Holmes, “A nonlinear oscillator with a strange attractor,” *Phil. Trans. R. Soc. Lond. A* **292**(1394), 419–448 (1979).
- ⁴I. Kovacic and M. J. Brennan, *The Duffing Equation: Nonlinear Oscillators and Their Behaviour* (Wiley, Chichester, 2011).
- ⁵M. Brennan, I. Kovacic, A. Carrella, and T. Waters, “On the jump-up and jump-down frequencies of the Duffing oscillator,” *J. Sound. Vib.* **318**(4–5), 1250–1261 (2008).
- ⁶T. W. Arnold and W. Case, “Nonlinear effects in a simple mechanical system,” *Am. J. Phys.* **50**(3), 220–224 (1982).
- ⁷B. Jones and G. Trefan, “The Duffing oscillator: A precise electronic analog chaos demonstrator for the undergraduate laboratory,” *Am. J. Phys.* **69**(4), 464–469 (2001).
- ⁸A. Li, L. Ma, D. Keene, J. Klingel, M. Payne, and X-j Wang, “Forced oscillations with linear and nonlinear damping,” *Am. J. Phys.* **84**(1), 32–37 (2016).
- ⁹E. H. Hellen and M. J. Lanctot, “Nonlinear damping of the LC circuit using antiparallel diodes,” *Am. J. Phys.* **75**(4), 326–330 (2007).
- ¹⁰Q. Xu, W. Fan, Y. Luo, S. Wang, and H. Jiang, “Nonlinear effect of forced harmonic oscillator subject to sliding friction and simulation by a simple nonlinear circuit,” *Am. J. Phys.* **87**(2), 116–124 (2019).
- ¹¹Y. Starosvetsky and O. Gendelman, “Vibration absorption in systems with a nonlinear energy sink: Nonlinear damping,” *J. Sound. Vib.* **324**(3–5), 916–939 (2009).
- ¹²R. Khosropour and P. Millet, “Demonstrating the bent tuning curve,” *Am. J. Phys.* **60**(5), 429–432 (1992).
- ¹³R. Dorner, L. Kowalski, and M. Stein, “A nonlinear mechanical oscillator for physics laboratories,” *Am. J. Phys.* **64**(5), 575–580 (1996).
- ¹⁴J. Tennenbaum, “Amplitude quantization as an elementary property of macroscopic vibrating systems,” *21st Century Sci. Technol.* **18**(4), 50 (2006).
- ¹⁵D. Penner, Y. B. Duboshinskii, D. Duboshinskii, and M. Kozakov, “Oscillations with self-regulating interaction time,” *Sov. Phys. Dokl.* **17**, 541 (1972).
- ¹⁶D. Doubochinski and J. Tennenbaum, “On the general nature of physical objects and their interactions, as suggested by the properties of argumentally-coupled oscillating systems,” e-print: [arXiv:0808.1205](https://arxiv.org/abs/0808.1205) (2008).
- ¹⁷V. Damgov and I. Popov, “Discrete oscillations and multiple attractors in kick-excited systems,” *Discrete Dyn. Nat. Soc.* **4**(2), 99–124 (2000).
- ¹⁸D. Cintra and P. Argoul, “Nonlinear argumental oscillators: A few examples of modulation via spatial position,” *J. Vib. Control* **23**(18), 2888–2911 (2017).
- ¹⁹Daniel Cintra and Pierre Argoul, “Non-linear argumental oscillators: Stability criterion and approximate implicit analytic solution,” *Int. J. Nonlin. Mech.* **94**, 109–124 (2017).
- ²⁰A. H. Nayfeh and D. T. Mook, *Nonlinear Oscillations* (Wiley, New York, 2008).
- ²¹Eugene I. Butikov, “Subharmonic resonances of the parametrically driven pendulum,” *J. Phys. A: Math. Gen.* **35**(30), 6209–6231 (2002).

- ²²P. L. Tea, “Pumping on a swing,” *Am. J. Phys.* **36**(12), 1165–1166 (1968).
- ²³S. Bae, “Equivalence of the pumping of a swing and the parametric resonance,” *Eur. J. Phys.* **27**(2), 291–298 (2006).
- ²⁴IYPT 2015 Problem 13: Magnetic pendulum. <<http://archive.iypt.org/problems/>>.
- ²⁵CUPT 2015 Problem 13: Magnetic pendulum. <http://pt.nankai.edu.cn/_upload/article/files/6f/3d/6c6ea34446f8aae250b942b3338c/b1e4a659-512b-4357-9ad2-9cd34bfc8356.pdf>.
- ²⁶W. G. Sihui Wang, *International Young Physicists' Tournament: Problems and Solutions 2015* (World Scientific, Singapore, 2018).
- ²⁷H. Strogatz, *Nonlinear Dynamics and Chaos* (Perseus Publishing, New York, 1994).
- ²⁸J. Maurer and A. Libchaber, “Effect of the Prandtl number on the onset of turbulence in liquid ^4He ,” *J. Phys. Lett.* **41**(21), 515–518 (1980).
- ²⁹E. Brun, B. Derighetti, D. Meier, R. Holzner, and M. Ravani, “Observation of order and chaos in a nuclear spin-flip laser,” *JOSA B* **2**(1), 156–167 (1985).
- ³⁰H. Gibbs, *Optical Bistability: Controlling Light with Light* (Elsevier, Orlando, FL, 2012).
- ³¹B. D. Aguda and B. L. Clarke, “Bistability in chemical reaction networks: Theory and application to the peroxidase–oxidase reaction,” *J. Chem. Phys.* **87**(6), 3461–3470 (1987).
- ³²T. Wilhelm, “The smallest chemical reaction system with bistability,” *BMC Syst. Biol.* **3**(1), 90 (2009).
- ³³D. Angeli, J. E. Ferrell, and E. D. Sontag, “Detection of multistability, bifurcations, and hysteresis in a large class of biological positive-feedback systems,” *Proc. Natl. Acad. Sci. U. S. A.* **101**(7), 1822–1827 (2004).
- ³⁴E. M. Ozbudak, M. Thattai, H. N. Lim, B. I. Shraiman, and A. Van Oudenaarden, “Multistability in the lactose utilization network of *Escherichia coli*,” *Nature* **427**(6976), 737–740 (2004).
- ³⁵F. Freyer, J. A. Roberts, R. Becker, P. A. Robinson, P. Ritter, and M. Breakspear, “Biophysical mechanisms of multistability in resting-state cortical rhythms,” *J. Neurosci.* **31**(17), 6353–6361 (2011).
- ³⁶J. F. Rhoads, S. W. Shaw, K. L. Turner, J. Moehlis, B. E. DeMartini, and W. Zhang, “Generalized parametric resonance in electrostatically actuated microelectromechanical oscillators,” *J. Sound Vib.* **296**(4–5), 797–829 (2006).
- ³⁷Here is an example to show how energy balance can be realized in a nonlinear driving oscillator. When a pendulum is driven by a linear driving force $a_0 \cos \Omega t$, then resonance occurs at $\Omega = 1$ and the amplitude goes to infinity without dissipation. If the driving force contains an additional term such as $(a_0 + a_2 x^2) \cos \Omega t$, then the average driving force will be dependent on amplitude. If the oscillation is nearly harmonic of the form $x \sim A \cos \Omega t$, we may approximate $x^2 = A^2 \cos^2 \Omega t$ as $(1/2)A^2$ by averaging it over one period. Then, the average driving force can be estimated as $(a_0 + (1/2)a_2 A^2) \cos \Omega t$. When a_0 and a_2 have opposite signs, the work done by the driving force obviously also has two opposite terms. When $A^2 = -2a_0/a_2$, the total work becomes zero, so energy balance is realized and the resonant amplitude is stabilized.



Cylinder Electrostatic Machine

There are three geometrical shapes possible for the production of electricity by rotating glass shapes against a “rubber”: the disk, the sphere and the cylinder. The cylinder type was developed by Edward Nairne (1726–1806). In this example at the Callan Museum at St. Patrick’s College in Maynooth, Ireland, the missing frictional rubber would be placed transversely on the upright glass insulator. This, and other apparatus from Maynooth, is described in Charles Mollan and John Upson, “The Scientific Apparatus of Nicholas Callan and other Historical Instruments” (Samton, Maynooth, 1994). The apparatus was photographed during two visits in 1998 and 1999. (Picture and text by Thomas B. Greenslade, Jr., Kenyon College)